

WIDEBAND SIMULATION OF EARTHQUAKE GROUND MOTION BY A SPECTRUM-MATCHING, MULTIPLE-PULSE TECHNIQUE

Alexander GUSEV¹ and Victor PAVLOV²

SUMMARY

To simulate earthquake ground motion, we combine a multiple-point stochastic earthquake fault model and a suite of Green functions. Conceptually, our source model generalizes the classic one of Haskell (1966). At any time instant, slip occurs over a narrow strip that sweeps the fault area at a (spatially variable) velocity. This behavior defines seismic signals at lower frequencies (LF), and predicts directivity effects. High-frequency (HF) behavior of source signal is defined by local slip history, assumed to be a short segment of pulsed noise. For calculations, this model is discretized as a grid of point subsources. Subsource moment rate time histories, in their LF part, are smooth pulses whose duration equals to the rise time. In their HF part, they are segments of non-Gaussian noise of similar duration. The spectral content of subsource time histories is adjusted so that the summary far-field signal follows certain predetermined spectral scaling law. The results of simulation depend on random seeds, and on particular values of such parameters as: stress drop; average and dispersion parameter for rupture velocity; rupture nucleation point; slip zone width/rise time, wavenumber-spectrum parameter defining final slip function; the degrees of non-Gaussianity for random slip rate in time, and for random final slip in space, and more. To calculate ground motion at a site, Green functions are calculated for each subsource-site pair, then convolved with subsource time functions and at last summed over subsources. The original Green function calculator for layered weakly inelastic medium is of the discrete wavenumber kind, with no intrinsic limitations with respect to layer thickness or frequency band. The simulation package can generate example motions, or used to study uncertainties of the predicted motion. As a test, realistic analogs of recorded motions in the epicentral zone of the 1994 Northridge, California earthquake were synthesized, and related uncertainties were estimated.

1. INTRODUCTION

Despite many studies addressed at the simulation of ground motion from a large earthquake, much is still to be done. In general, to simulate earthquake ground motion from a known fault, one should be capable to simulate both (1) fault/source space-time evolution, and (2) wave propagation from the fault to a receiver. The last step may include such separate substeps as (2a) propagation of linear wave up to the bedrock under the site/receiver, and (2) non-linear propagation in weaker upper layers. We confine our study by (1) and (2a); moreover, in (2a) we use simple, horizontally layered, model of Earth structure.

Two general approaches have been developed to describe space-time evolution of earthquake source. One is based on the elastodynamic representation of a fault, and treats a fault as a dislocation/crack. While this approach is conceptually attractive, in most its realizations it fails to predict an important property of the fault motion – localization of slip process in a narrow running strip (Haskell 1966; Heaton 1990). It also cannot predict realistically high-frequency (HF) part of wide-band spectrum of source radiation. Another approach is to use semi-empirical models, that combine some theoretical reasoning with generalization of empirical data. In this line,

¹ *Institute of Volcanology and Seismology FEB RAS*, 9 Piip Blvd, 683006 PETROPAVLOVSK-KAMCHATSKII, Russia;
Email : gusev@emsd.iks.ru

² *Kamchatka Branch, Geophysical Service RAS*, 9 Piip Blvd, 683006 PETROPAVLOVSK-KAMCHATSKII, Russia;
Email : pvm@emsd.iks.ru

most important steps are: the concept of Haskell(1966)-Aki(1967) of approximate self-similitude of earthquake sources and of spectral scaling law; the proposal of Aki(1967)-Brune(1970) of simple omega-square spectral scaling law with self-similitude; demonstration of lack of self-similitude in actual wideband spectral scaling (Gusev 1983); derivation of properties and parameters of strong motion based on spectral scaling law, both assuming similitude and using point source model (Hanks&McGuire1981) and assuming wideband semi-empirical finite source models with no spectral similitude (Gusev 1983, Papageorgiou&Aki 1983). In a number of studies, a source of a large earthquake was represented as a composition of earthquake sources of smaller size (Boatwright 1982, Papageorgiou&Aki 1983, and later work). (It should be mentioned that this line of study is based on a disputable assumption, that such composition is meaningful from the tectonophysical viewpoint.) For fault-to-site distances comparable or exceeding fault width, these approaches have produced some useful techniques for ground motion simulation. However, these approaches essentially fail to solve the problem of prediction of ground motion at small distances where realistic details of space-time evolution of a large event become critical.

The main difficulty, in our view, is the need to comply simultaneously with the following two critical requirements: (1) the low-frequency component of simulated signal must incorporate our knowledge of details of real fault propagation, first of all the running strip model of Heaton (1990) and final slip structure anticipated by Andrews 1980 and refined by Sommerwille et al. (1999); (2) the high-frequency component is to follow our empirical knowledge of typical Fourier spectra at moderate-to-large distances, and also to emulate non-Gaussian amplitude statistics of observed near-fault records (Gusev 1996). Our approach, presented below, is aimed to satisfy, systematically, both these groups of requirements. This is performed in two consecutive steps: first we generate a source with unrealistic, nearly-white-noise high-frequency signal but accounting for all important details of low-frequency behavior, of envelope structure and of statistics of peaks; then we smooth the source signal in an accurately controllable manner, fitting an empirical spectral scaling law (i.e., in essence, an empirical acceleration spectral trend).

The presented simulation procedure is aimed at a realistic prediction of earthquake ground motion for the magnitude range $M_w=5-9$, the hypocentral distance range 5-400 km and frequency band 0.03-25 Hz. The earthquake source is represented as a set of point sources with appropriate time histories. For any site in question, and for each subsource, we calculate medium response to a unit step in seismic moment for a point dislocation (“Green function” loose sense) and convolve it with the respective time history. Such contributions of all subsources are added up, to result in a synthetic ground motion. Correspondingly, the entire simulator procedure consists of the source simulator module, the Green function calculator module, and the convolver module that performs convolution in time, and summation over subsources. We use an original Green function calculator for layered medium, accurate over entire relevant frequency band, from static terms (“swing”) to very high frequencies. To illustrate capabilities of the proposed method we simulate near-source ground motion of a well-recorded earthquake, and analyze the uncertainty of the simulation.

2. THE TECHNIQUE FOR THE SIMULATION OF STRONG GROUND MOTION

2.1 Source simulator

The source simulator algorithm generalizes the classic Haskell (1966) stochastic fault model that assumes that at a particular point, the process of slip is of definite duration, denoted “rise time”. Haskell also proposed that the slip velocity, viewed as a function of space and time, is a random function. We follow these two assumptions, but introduce the following modifications:

1. Instead of the Haskell’s fault with a constant final slip, a variable, random final slip is assumed, governed by the power spectrum that is a power-law with respect to wavenumber. This kind of wavenumber spectrum was proposed by Andrews (1980) and confirmed by Sommerwille a.o. (1999) based on empirical data.

2. Kinematics of Haskell’s source is generalized in the following way: the rupture front is of a general shape (not a straight line); the nucleation point is arbitrary; and the rupture velocity is variable, with a prescribed mean (not a constant).

3. Instead of Haskell’s omega-cube far field spectrum, the far-field spectrum of a simulated source is adjusted, in its high-frequency part, to a particular spectral shape derived from a preset regional spectral scaling law.

This general concept is to be realized in a numerical scheme. Following in many respects (Gusev 1983) we introduce a grid of point-like dislocation subsources. Each subsource possess a fraction of the total seismic moment of the source, and the distribution of seismic moment over subsources is governed by the aforementioned ran-

dom final slip function. The duration of a subsurface is defined first of all by the value of rise time (the duration of local slip), assumed the same over entire fault in the current version of the algorithm. This duration is somewhat increased additionally, to account for the finite size of the fault cell represented by a point subsurface. Each subsurface has an individual, random moment rate time history. In absolute time, subsurfaces are switched on by the arrival of the rupture front, otherwise their time histories are uncorrelated. At present, we ascribe no direct physical meaning to individual point subsurfaces; they serve only as a tool for numerical simulation of an incoherent source with mostly uncorrelated spots. The number of subsurfaces can be large (a 50×25 grid is quite acceptable). However, the assumed complete lack of correlation among time histories of subsurfaces may become inadequate for a very dense grid. For this reason, the model may overpredict high-frequency amplitudes when used at a too small distance from a fault. A rough estimate of the minimum fault distance is about (fault length)/20, or 5 km for a 100-km fault. The above considerations led us to the simulation procedure that consists of the following steps:

1. Specification of parameters of the model. These include common source parameters like seismic moment, stress drop, nucleation point position, rise time and mean rupture velocity. The fault shape is assumed to be rectangular, length $L \times$ width W . The values of L and W can be either preset or calculated from $L(M_w)$ correlation relationship adjusted for stress drop, assuming M_w -dependence of the aspect ratio. Also, parameters of the numerical model are set, namely: the subsurface numbers along L and W , and time step. In the current version, strike, dip and slip angles of subsurfaces are identical.

2. Monte-Carlo simulation of the final slip distribution. This simulation departs from generating 2D random white Gaussian spectrum that represents logarithm of slip in wavenumber domain. Then isotropic power-law filter is applied; its exponent s is preset. The result is passed to coordinate domain, and rescaled to acquire the preset value of rms deviation, equal to CV_{xy} . Then, the obtained function is exponentiated, resulting in everywhere positive random function with lognormally distributed values. At last, a finite portion of the produced 2D field is cut out by an appropriate 2D taper (“cap”) function, nonzero over a L by W rectangle. If a side of a fault cuts the free surface, tapering is switched off along it. The value of CV_{xy} defines how heavy-tailed shall be the distribution of values of the simulated final slip. At $CV_{xy}=0$, the constant-final-slip case is simulated. Technically, CV_{xy} is near to the coefficient of variation for slip values. See Fig. 1 for an example of simulated final slip.

3. Monte-Carlo simulation of the rupture propagation history. In the simplest mode, rupture front is assumed to be circular and to move in steps of identical length, smaller than the size of a subsurface cell. At the i -th step, the value v_i of rupture velocity is determined as a product of the preset mean value v_m , and of a random number drawn from uniform distribution in the range $(1-DV, 1+DV)$, where DV is another preset parameter. In a more advanced mode, the front propagation history is controlled by 2D distribution of random values of rupture velocity. For an example of simulated rupture front propagation see Fig. 1.

4. Monte-Carlo simulation of “skeleton” time histories for subsurfaces. For each subsurface, its “skeleton” time history is a provisional version of its moment rate function. It is a random sequence of delayed positive delta-like pulses (spikes), with appropriate amplitude statistics, and appropriate envelope (boxcar or “cap-like” or other). Essentially, it is a segment of modulated positive white noise. Inter-pulse delays are random, and the sequence of pulse onsets is nearly Poissonian. The amplitude statistics of spikes is lognormal. By selection of the parameter CV_i of the lognormal law, one can define whether the resulting accelerograms will appear like Gaussian noise or will look “spiky” to a certain controllable degree. For each subsurface, the onset time of a sequence is determined by the arrival time of the rupture front to this subsurface. The duration of the envelope (and thus of a sequence) is determined by the value of the rise time. From the tectonophysical viewpoint, each delta-like spike can be related to a failure of a single small asperity (Gusev 1989). The heavy-tailed statistics of spike amplitudes is needed to emulate heavy-tailed, non-Gaussian statistics of acceleration peaks (Gusev 1996); such a behavior is presumably the manifestation of the heavy-tailed distribution of the fault strength and local stress drop. The complete set of “skeleton” time histories of subsurfaces represents a “skeleton source”. For illustration see Fig. 1 and 2.

5. Creating the “dressing operator”. At this point, low-frequency behavior of the source is already constructed. As for its high-frequency component, its envelope and peak statistics have also been simulated. The only problem is the unrealistically high spectral amplitudes at high frequencies, i.e., above $(4-6) \times$ (corner frequency). To rectify this deficiency, we apply to skeleton time functions a specially designed “dressing operator”. In time domain, it reduces to smoothing, by convolution with a pulse with unit integral, or, shortly, “unit pulse”. To construct the dressing operator we first calculate the source spectrum (Fourier spectrum of the moment rate time

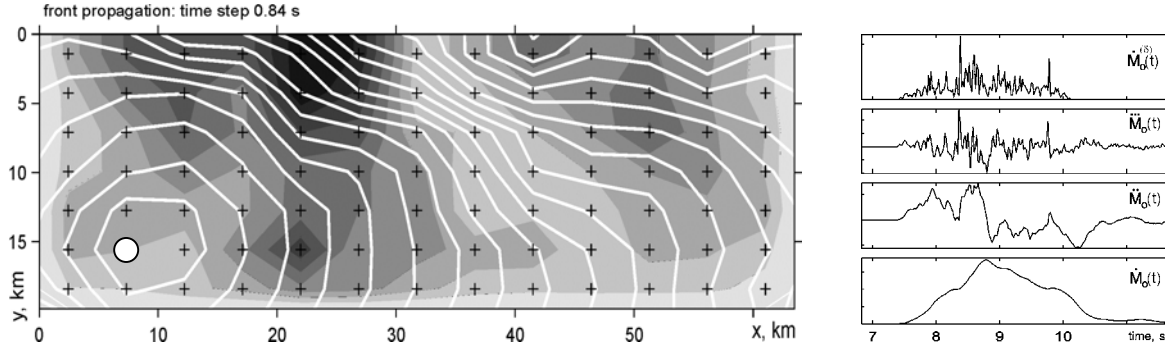


Figure 1: Left: an example of 2D final slip function, shown as density. Fault parameters: $M_w=7.2$, $L = 63$ km, $W=20$ km. Subsource grid 13×7 (crosses). Random slip follows isotropic $k^{-1.5}$ wavenumber amplitude spectrum. 2D taper function used over three sides; upper side ($y=0$) is assumed to cross the Earth surface. White dot is the nucleation point. White contours are successive rupture front positions, simulated kinematically from random rupture velocity field. Right: time histories associated with a particular subsource. Skeleton time history is the upper trace. Three other traces are $\dot{M}_0(t)$, $\ddot{M}_0(t)$ and $\overset{(s)}{M}_0(t)$; they represent subsource contribution to far-field body wave acceleration, velocity and displacement, respectively.

history of an equivalent point source) that corresponds to the time history of constructed “skeleton” source (obtained by stacking all subsources). We then compare the result with the preset “target” source spectrum, derived from the regional spectrum scaling law (that is, ultimately, from averaged observed spectra) for the given values of moment magnitude and stress drop. The ratio of these two spectra, smoothed and somewhat modified, gives us the module of the “dressing operator” in frequency domain. Its phase spectrum is adjusted so as to make its time-domain representation causal (minimum-phase). This procedure is illustrated on Fig. 3.

6. “Dressing the skeleton”. The dressing operator (i.e., convolution with unit pulse) is applied to “skeleton” time histories of subsources, giving a final set of individual moment rate time histories of subsources. The spectrum of their sum, in its high-frequency part, approximates the “target” spectrum in the rms sense. In time domain, the same sum gives the shape of the far-field body wave displacement signal for a ray normal to the fault. Similarly, using for convolution first and second derivatives of the unit pulse (seen in Fig. 3), one obtains the shapes of far-field velocity and acceleration signals, as illustrated in Fig. 1 for an individual subsource.

The described source simulation algorithm is capable of producing realistically-looking far-field and near-field ground motions. In particular, it reproduces well the common directivity effects. Also, it successfully emulates, in terms of amplitude levels, observed peak accelerations and velocities, as well as response spectra and characteristic durations. However, the described procedure has a significant deficiency: its repeated runs generate signals whose amplitudes and response spectral levels vary only slightly from run to run; in other words, their variability is unrealistically low. The evident cause is that the simulated spectrum is too close to the mean/target one, because of the feedback loop inherent within the described procedure. Indeed, it is designed to adjust far-field Fourier spectral amplitudes of an individual simulated earthquakes to similar *mean* amplitudes at each frequency. This feedback strongly dampens the natural variability of signals: output spectral amplitudes generated in successive runs of the procedure are automatically kept within a too narrow corridor. The case of such an unrealistically perfect spectral fit is given on Fig. 3 and well seen on Fig 3c. To overcome this problem, we must disconnect the feedback loop, thus setting the purely-random/fluctuational component of variability of ground motion to the correct degree.

Towards this end, the above algorithm was modified in the following way. Instead of calculating the “dressing operator” of the Step 5 through individual fit at each simulation run, it is calculated only once. At a preliminary stage, we repeat the simulation many (25) times with all parameters fixed, changing only the random seeds, and then average the (amplitude) spectral correction functions obtained in each run. From this average spectral correction we construct the average “dressing operator”, and “freeze” it. Afterwards, simulation proper is performed, single or multiple, with “frozen” correction operator and no feedback. After such a modification, the algorithm generates signals with realistic variability. These are adequate for such uses as: generating suites of design earthquake ground motion, studying its sensitivity to variations of input parameters of the model, and/or analyzing variability/uncertainty of the result.

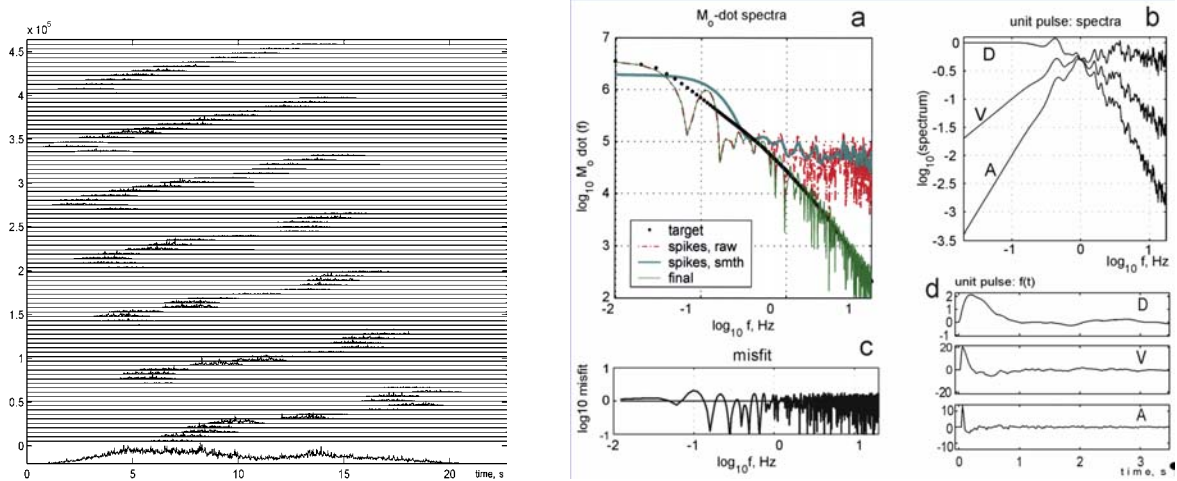


Figure 2: Skeleton time histories for 91 subevents of the source of Fig. 1. The lowermost trace is the sum over subsources.

Figure 3: Spectral fitting for the discussed example case. *a*: a set of $\dot{M}_0(f)$ spectra (in 10^{20} dyne cm units) that represent: target spectrum, spectrum of the skeleton time function (sequence of spikes), its smoothed version, and final spectrum. *b*: Amplitude spectral representation for “dressing operator”; multiplication by spectrum D converts the skeleton spectrum to the final $\dot{M}_0(t)$ spectrum, using spectra V and A , one can, similarly, perform conversion to $\ddot{M}_0(t)$ and $\dot{M}_0(t)$. Spectrum D is obtained by division of target spectrum of by smoothed skeleton spectrum (see graph *a*). At frequencies above $0.2 \times (\text{corner frequency})$ it is set to unity. *c*: spectral misfit between target spectrum and final spectrum of graph *a*. *d*: time function representation of the “dressing operator” or unit pulse, see graph *b* for corresponding amplitude spectra.

2.2 Green function calculator, convolution module and attenuation correction

To match the level of accuracy promised by the source simulator described above, an accurate wideband Green function calculator was needed. We use the original discrete wavenumber code that calculates pulse response of the layered elastic medium to a step-like double-couple source. The code is based on the advanced version of the method of Alekseev and Mikhailenko (1980), developed recently by Pavlov (2001). The solution is initially represented, in cylindrical coordinates, as an integral sum over surface vector harmonics. Alekseev and Mikhailenko (1980) introduce a distant boundary and convert the integral representation into a series over discrete wavenumbers that are roots of a certain equation related to Bessel functions. To determine coefficients of this series, for each frequency-wavenumber pair one must solve ordinary differential equations in depth coordinate (a single equation for the SH case and a pair of coupled equations for the P-SV case). Right-hand parts of these equations are corresponding coefficients for the expansion of the point source. These differential equations are solved analytically by means of the “auxiliary functions” first introduced by Fatyanov and Mikhailenko (1988). For SH waves, an auxiliary function is the scalar function of depth such that the depth derivative of the SH potential is equal to the product of the auxiliary function and the potential. For the P-SV case, the auxiliary function is similar and forms a 2×2 matrix. Auxiliary functions, and displacement and stress coefficients are calculated by closed analytical formulas. The main advantage of this method is the lack of numerical instability inherent for propagator methods, because in the auxiliary function method, all relevant exponential factors are below unity by absolute value. To ensure uniformly the preset level of numerical accuracy, the number of terms in the series is selected adaptively. The developed numerical method provides an accurate broad-band representation of ground motions in a layered medium. It has no intrinsic limitations with respect to the layer thickness and bandwidth, and predicts both so named “swing effect” at zero frequency, and high-frequency body wave spikes equally well.

In the convolution module, for each site, the first step is to convolve over time the subsurface time histories and the corresponding subsurface Green functions. The second step is to add thus obtained contributions of all subsources, resulting in the ground motion at the site. This is repeated for each site. In addition, attenuation corrections (through “kappa” factor and distance-dependent term) are added here. Alternatively, a frequency-independent Q profile can be included in the main procedure for Green function calculation. The option of frequency-dependent Q profile is under development.

2.3 Parameters of the model

We give below the list of most important parameters that define a particular realization of our numerical model. Parameters can be selected/modified to attain such aims as: (1) tuning both the source model and the model of the medium to a particular seismological situation; in order to tune the model, particular values of parameters are selected; (2) analyzing the variability and uncertainty of the predicted motion, both purely random and parameter-related; and (3) generation of a suite of representative ground motions. Random variability related to intrinsically stochastic part of the model is simulated by using a series of sets of random seeds. To deal with random variability related to the natural variability of input parameters, there are two ways. First, one can generate random values of input parameters (by drawing random numbers out of appropriate random distribution(s)), use these as input for simulations, and at last analyze the variability of resulting ground motion parameters. Second, one can suppose that the distribution of an input parameter, (say, “ b ”), is known, and derive distribution of an output parameter (say, “ a ”), using sensitivity (i.e., derivative da/db). We shall use this latter procedure. (Being simpler, it is less general, as it works only for the cases of weak nonlinearity and independent parameters.)

Now we list the most important parameters of the model:

A. Parameters of earthquake source/fault and of regional seismicity.

1. General.

- 1.1. Geographic coordinates φ_c , λ_c and depth H_c for the center of fault rectangle .
- 1.2. Moment magnitude M_w ; strike, dip and rake angles.
- 1.3. Stress drop parameter δ , defined as logarithmic deviation of individual stress drop value from its regional average ($\delta = \Delta \log \Delta \sigma$).
- 1.4. Length L and width W of the fault rectangle; numbers of subsources: n_L along L and n_W along W

2. Kinematics and dynamics.

- 2.1. CV_{xy} : defines how strongly oscillating (non-Gaussian) will be the simulated final slip function.
- 2.2. The exponent s in the power law that defines the power spectrum ($\propto k^{-s}$) of the final slip.
- 2.3. Location of the nucleation point x_n , y_n along L and W , or its world coordinates φ_n , λ_n and H_n .
- 2.4. Rupture velocity parameters: mean value v_m , half-range dv_r of random perturbation of mean value of rupture velocity; relative range DV of random perturbation of instant value of rupture velocity
- 2.5. Rise time T_{rise}
- 2.6. CV_t : defines the degree of non-Gaussian behaviour (“spikyness”) of accelrograms.

4. Random seeds

- 4.1. Random seed defining the final slip function.
- 4.2. Random seed defining the time histories of subsources.
- 4.3. Random seed defining the perturbation of the mean value of rupture velocity.
- 4.4. Random seed defining the random history of rupture velocity
- 4.5. Random seed defining the perturbation of the nucleation point position.

5. A particular scaling law ($\dot{M}_0(f | M_w)$) for source spectra, tabulated or in an analytical form.

B. Parameters of the layered medium and of a site.

1. The site position.

2. The velocity-density column for a site (includes top depth, ρ , V_P , V_S , and maybe Q_P and Q_S for each layer.

3. The value of kappa parameter for a site (site-specific upper layer attenuation), and $Q(f)$ vs. distance.

In the case of a non-standard value of stress drop, spectral scaling law is modified correspondingly, using the δ parameter to squeeze or stretch the spectral shape along frequency axis (as proposed by G. Panza). In the present version of the algorithm, two particular spectral scaling laws are preset: for W.USA shallow earthquakes, Joyner (1984) modification of Brune (1970) scaling law (assuming similitude); and semi-empirical scaling law of Gusev (1983), with no similitude.

3. AN EXAMPLE CASE: NORTHRIDGE 1994 EARTHQUAKE

An appropriate test for the algorithm described above is its application for emulation of a set of records obtained in the epicentral zone of a large earthquake on various ground types. To perform such a test, 18 near-source records of $M=6.7$, 1994, Northridge, California, earthquake were simulated (see Fig. 4 for the general overview of the fault and recording stations). To fix the parameters of the source model and of the layered media associated with local geology under stations we widely used the published results of source inversion after Wald

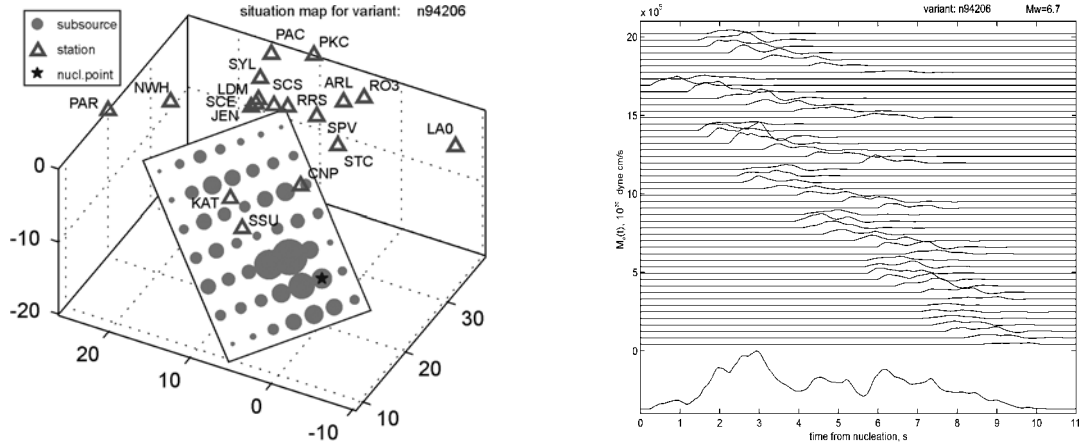


Figure 4. Left: perspective view of source rectangle and receivers/stations for the $M_w=6.7$ Northridge 1994 event. Subsources indicated as dots whose size reflects its seismic moment as used in the variant #206. Star is the nucleation point. Coordinates in km. Right: Moment rate time functions for 49 subsources of variant #206 of a simulated Northridge earthquake, and also the summary moment rate function (below).

et al. (1996). The only parameter whose values were fit to real data is the kappa parameter. In Table 1 we give source parameters used in our simulation; most of them are adapted from (Wald et al, 1996). For other parameters, comments are given below. As for the particular scaling law of source spectra used in simulation, we used Brune’s omega-square law, that is valid the case of Western USA, in the modification of Joyner (1984).

Table 1. Assumed values for fault parameters that were used for simulation

φ_c	λ_c	H_c	Strike	dip	rake	M_w	L	W	n_L	n_W
34.28°	-118.56°	12.5 km	122°	40°	101°	6.7	18 km	24 km	7	7

v_m	T_{rise}	φ_n	λ_n	H_n	δ^*	DV^{**}	CV_t^{***}	$CV_{xy}^\#$	$s^{##}$
3 km/s	0.7s	34.35°	-118.54°	17 km	0.15	0.8	0.5	0.5	1.5

* $\delta=0.15$ means that stress drop is 1.4 times above the regional average; based on the value of Ward et al (1996), equal to 74 bar, compared to the reference value of 50 bar for the Brune-Joyner spectral model.

** A guess, our results suggest that it is probably too low.

*** A tentative value based on our experience with simulation, a trade-off between “dull” Gaussian-noise type accelerograms and expressedly non-Gaussian records with seemingly too prominent individual spikes.

A similar tradeoff between nearly-constant slip at $CV_{xy}=0-0.2$ and very expressed “asperities” at $CV_{xy}>0.8$.

Andrews (1980) proposed $s=2$; we found that this value results in seemingly too scarce high wavenumbers, and somewhat decreased it. The estimate, $s=1.75$, of Sommerwille et al (1999) is close to our assumption.

As for the model of the medium, Wald et al.(1996) give vertical profiles for stations with “rock” and “soil” geology. We used them to calculate Green functions for stations whose ground was specified as “rock” and “deep soil”/“basin”. For two stations with intermediate ground conditions, we used an “intermediate” structure, with “interpolated” velocity profile. Distance-dependent attenuation term was omitted in this simulation. Kappa values were set as 0.04, 0.05 and 0.075 s for rock, intermediate and soil stations, respectively. They were adjusted during simulation. Among them, the value 0.075 s for soil may look too large; in fact, this value seem to reflect correctly the non-linear enhancement of attenuation in a soft soil in the epicentral zone.

To select an example of simulation, we had some freedom because we could look through many variants of random seeds, making our demonstration example less convincing. Actually, we looked through only ten variants, to select two ones (#206 and #300) that show ground motion parameters quite near to the observed ones. For variant #206, we show moment rate functions for subsources on Fig. 4. For combined far-field motion for entire source see Fig. 5. To compare simulated and observed time histories of ground motion at five representative stations see Fig. 6. The general appearance and amplitudes match acceptably; however, the observed motion at rock stations is somewhat more spiky (non-Gaussian) than the simulated one. To generate the mentioned ten variants, we changed independently three random seeds that define: 2D final slip function, subsurface time functions, and rupture front time history, respectively.

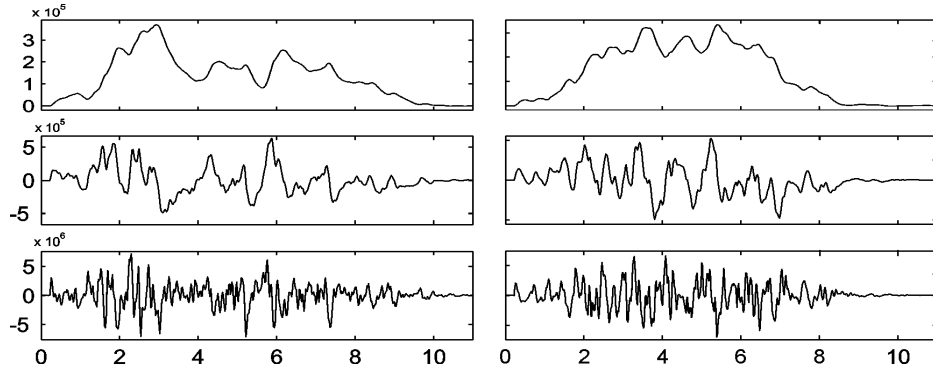


Figure 5. Far-field source time functions for the variants #206 (left) and #300 (right). Top to bottom: functions $\dot{M}_0(t)$ (moment rate), $\ddot{M}_0(t)$, and $\dddot{M}_0(t)$ in 10^{20} dyne cm/s, 10^{20} dyne cm/s², and 10^{20} dyne cm/s³ units.

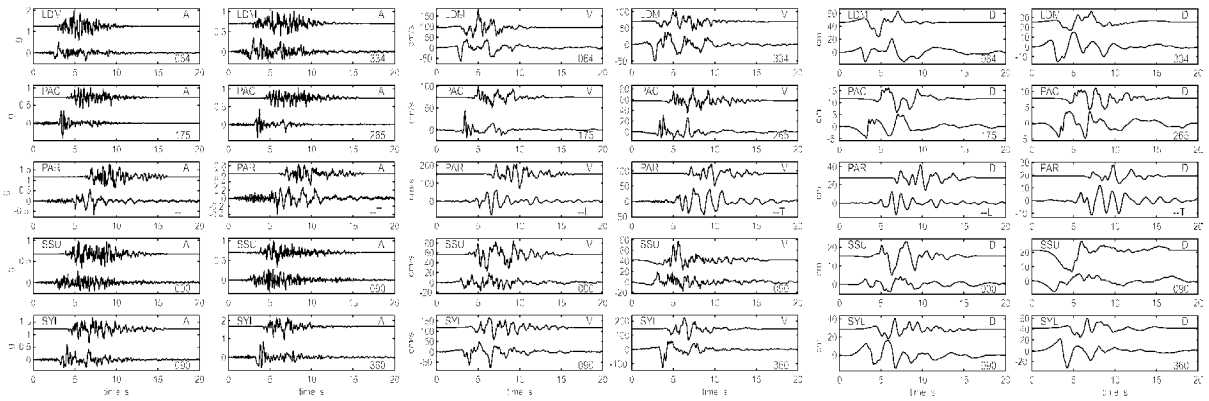


Figure 6. Comparison of observed and simulated (variant #206) time histories for acceleration (left), velocity (center) and displacement (right) for five stations, for two horizontal components. In each box, the lower trace is observed and the upper trace is simulated. Stations shown, top to bottom: PAC and LDM (rock); PAR, SSU and SYL (deep soil/basin, widely different azimuths from epicenter).

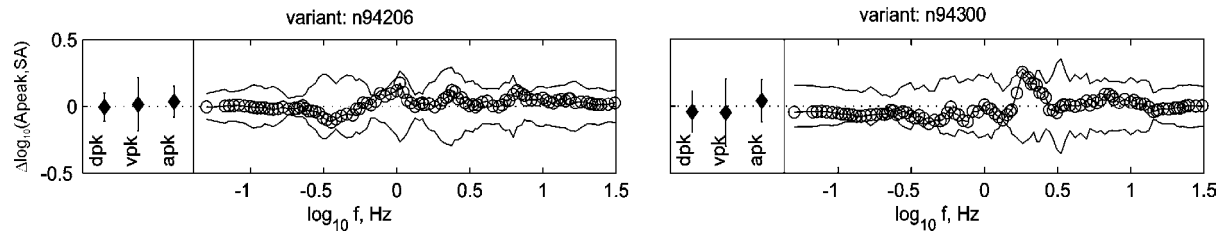


Figure 7. The misfit of horizontal peak and spectral amplitudes over 18 stations, for two simulated variants: #206 and #300. Misfit values are the differences (simulated minus observed) between \log_{10} peak displacements, velocities and accelerations (left box in each graph), and for \log_{10} pseudo response accelerations (right box). For all differences, average values over two horizontal components are shown. Standard deviations over 18 stations for the same data are shown, as error bars for amplitudes, and as a corridor around zero level for spectra.

Let us now consider the differences between simulated and observed time functions. (Observed functions were rotated and filtered to match the recorded ones). We analyze these differences in the form of logarithmic amplitude misfit, denoted generally as $\Delta \log_{10}(A) = \log_{10}(A(\text{simulated})) - \log_{10}(A(\text{observed}))$. The misfit was determined for pseudo response acceleration PRA ($\Delta \log_{10}(\text{PRA})$) calculated over 25 frequencies between 0.1 and 20 Hz, and also for the peaks of acceleration, velocity and displacement, and averaged over the two horizontal components and over 18 stations. On Fig. 7, one can see $\Delta \log_{10}(A)$ for the two “better-fitting” out of 10 simulated variants. The average misfit over 10 variants and 25 frequencies is less than 0.03 (7% in A); and rms deviations of amplitude residuals among stations are about 0.17 \log_{10} units. On the whole, the results of comparison can be considered as quite satisfactory. Bazurro et al.(2004) studied how well the results of our simulation, and also of six

more techniques for simulation of ground motion can emulate linear and especially non-linear response of single degree of freedom system to the observed motion of the 1994 Northridge earthquake. The technique described above was the only one that produced realistic results over entire analyzed frequency band (0.25-10 Hz).

4. UNCERTAINTY ANALYSIS

The developed simulation technique was also applied to estimation of uncertainty of the predicted ground motion for 1994 Northridge earthquake on the same 18 stations. The effects of factors contributing to uncertainty were analyzed in the following manner. The five following source-related factors were treated as random ones, and were analyzed directly in terms of rms deviation of the $\log_{10}(A)$, denoted σ_{log} : (1) random seed defining final slip distribution over the fault; (2) random seed defining subsurface time histories; (3) random seed defining random variations of instant rupture velocity; (4) the random value of mean rupture velocity, considered to be distributed uniformly within the range 2.16-3.24 km/s (Mach number 0.6-0.9); and (5) the random position of nucleation point, considered to be distributed uniformly over the lower third of the fault area (note that though the latter assumption seems to be reasonable, it significantly suppresses possible effects of variations in directivity). For these factors, σ_{log} was determined from dispersion of results over 16 tries.

Another set of six source-related factors, all parametric, was analyzed using sensitivity approach. In the following list of factors, after each item, we give *in brackets* the value of sensitivity ($d\log_{10}(A)/d(\text{parameter})$). For the lack of space, we cite only averages over all 25 analyzed frequencies. In cases of expressed non-linearity, minimal estimate is taken. The assumed rms deviation of a parameter is then listed *in braces*. (6) Stress drop $\Delta\sigma$. This parameter affects amplitudes through changes in Fourier spectral level, and in signal duration related to fault size. During variation of $\Delta\sigma$, fault center was fixed. [$d\log_{10}(A)/d(\log_{10}\Delta\sigma)=0.32$]{0.1}. (7) Coefficient of variation CV_t for amplitudes of delta-like spikes. [0.19]{0.15}. (8) Coefficient of variation CV_{xy} for the values of final slip distribution. [0.091]{0.15}. (9) The exponent s in the power law that defines the power spectrum of the final slip. No clear effect was noted for the range $s=1.0$ -2.2. (9) The range of variations for the rupture velocity DV . Again, no clear effect was noted for the range $DV=0.0$ - 1.0; probably the assumed range for DV is unrealistically small. (10) Seismic-moment-related uncertainty was estimated from theoretical considerations; for LF range: [$d\log_{10}(A)/d\log_{10}(M_0)=0.5$ -0.67]; for HF range: [$d\log_{10}(A)/d\log_{10}(M_0) = 0.2$ -0.3]; this factor was not included into further calculations. A few more factors were included that are external to the source; their analysis is much less interesting because their effect strongly depends on the particular geometry of the fault and on the station set, and thus is of low generality. Among these factors, only dip angle and H_c were found to be significant. (11) Dip angle, degrees. [0.024]{10°}. (12) H_c , km. [0.045]{2.5}. For factors 6-12, σ_{log} was determined as a product of sensitivity and assumed rms deviation of a factor. Uncertainty related to deviations from a regional spectral scaling law was ignored.

The results are listed in Table 2, for mean PSA (line ‘‘A’’), for PSA averaged over bands: 0.1 to 0.3 Hz (‘‘XL’’), 0.31 to 1.5 Hz (‘‘L’’), 1.51-5 Hz (‘‘M’’) and 5.1-20 Hz (‘‘S’’), and for peaks of acceleration (‘‘a’’), velocity (‘‘v’’), and displacement (‘‘d’’). In the header line numbers of factors are given, as used in the last paragraphs. Column S_f lists joint rms deviation calculated assuming independence of effects of the analyzed factors; this assumption seems to be reasonable to a certain degree. Column S_{is} lists interstation rms deviation of amplitudes in a particular simulation variant, averaged over 10 variants of Section 3, these values give an empirical estimate of uncertainty related to a ‘‘random’’ selection of a site of a certain (definite) ground type. Column S_{tot} is obtained through

Table 2. Uncertainties shown as rms deviations of $\log_{10}A$, related to individual factors, and to joint effects

	(1)	(2)	(3)	(4)	(5)	(6)	(7)	(8)	(11)	(12)	S_f	S_{is}	S_{tot}
A	0.047	0.021	0.042	0.066	0.031	0.031	0.028	0.013	0.045	0.024	0.11	0.17	0.21
XL	0.057	0.029	0.072	0.108	0.070	0.041	0.006	0.011	0.038	0.041	0.15	0.18	0.24
L	0.056	0.047	0.058	0.084	0.034	0.037	0.027	0.009	0.045	0.021	0.14	0.22	0.26
M	0.040	0.044	0.025	0.058	0.017	0.023	0.038	0.010	0.045	0.005	0.09	0.18	0.21
S	0.051	0.025	0.030	0.042	0.022	0.025	0.033	0.020	0.041	0.021	0.09	0.14	0.17
a	0.054	0.026	0.047	0.052	0.027	0.031	0.035	0.009	0.057	0.015	0.10	0.14	0.18
v	0.051	0.042	0.064	0.079	0.048	0.041	0.027	0.015	0.053	0.033	0.13	0.12	0.18
d	0.061	0.025	0.068	0.067	0.075	0.038	0.013	0.015	0.045	0.034	0.14	0.18	0.24

summation of variances related to columns S_f and S_{is} , it gives our estimate of total uncertainty. Note that all the analysis above is based on rms averages of A values of two horizontal components.

The most important single factor in uncertainty is the station-related term, manifesting mostly site geology effects and path-related effects like “focusing” etc, but including (probably minor) effect of all direction-related factors unexplained by the simulation procedure. Among other factors, the group of random seeds representing intrinsic model uncertainty and the group of parametric factors seem to make approximately equal contributions. Among random seeds, the contribution of mean rupture velocity (treated as a random factor) is the largest, representing its importance in forming the directivity effects. Second in this group is the contribution of random final slip distribution over fault area. As for absolute values, our estimates of uncertainty are based mostly on assumptions of minimum uncertainty of parameters, and thus must be treated as “optimistic” or “less conservative”.

5. ACKNOWLEDGEMENTS

Authors are indebted to Giuliano Panza who proposed and supported this study. Discussions with him, Fabio Romanelli and Franco Vaccari were highly valuable. Analysis of uncertainty was proposed and facilitated by Organizing Committee for Treasure Island prediction exercise; they also kindly provided station characteristics and preprocessed observational data.

6. REFERENCES

- Aki, K. (1967) Scaling law of seismic spectrum: *J. Geophys. Res.* 72, 1217-1231.
- Alekseev A.S, Mikhailenko B.G. (1980), The solution of dynamic problems of elastic wave propagation in inhomogeneous media by a combination of partial separation of variables and finite-difference method. *J. Geophys.* 48, 161-172.
- Andrews, D. J. (1980) A stochastic fault model. 1. Static Case. *J. Geophys. Res.*, 78, p. 3867-3877.
- Bazzurro, P., Sjöberg, B., & Luco, N. (2004) Post-Elastic Response of Structures to Synthetic Ground Motions, Tech. Rep. AT2, for PEER Lifelines Program project 1G00, *AIR Worldwide Co.*, San Francisco,
- Brune, J. N. (1970). Tectonic stress and the spectra of seismic shear waves from earthquakes, *J. Geophys. Res.* 75, 4997–5009.
- Fatyanov A.G., Mikhailenko B.G., (1988), A method for calculating non-stationary wave fields in anelastic layered media. *Doklady AN SSSR*, 301, 834-839. (In Russian).
- Gusev A.A. (1983), Descriptive statistical model of earthquake source radiation and its application to an estimation of short-period strong motion. *Geophys. J. Roy. Astr. Soc.*, 74, 787-808.
- Gusev A.A., (1989), Multiasperity fault model and the nature of short-period subsources. *Pure Appl. Geophys.*, 130, 635-660.
- Gusev, A.A. (1996), Peak factors of Mexican accelerograms: evidence of non-Gaussian amplitude distribution. *J. Geophys. Res.* 101, 20083-20090.
- Hanks, T. C., and R. K. McGuire. (1981). The character of high-frequency strong ground motion, *Bull. Seism. Soc. Am.* 71, 2071–2095.
- Heaton, T.H., 1990. Evidence for and implications of self-healing pulses of slip in earthquake rupture. *Phys. Earth Planet. Inter.*, 64: 1-20.
- Haskell, N.A., (1966), Total energy and energy spectral density of elastic wave radiation from propagating faults. II. A stochastic fault model. *Bull. Seism. Soc. Am.*, 56, 125-140.
- Joyner, W.B., (1984), A scaling law for the spectra of large earthquakes, *Bull. Seism. Soc. Am.*, 74, 1167-1188.
- Pavlov V.M. (2002) A convenient technique for calculating synthetic seismograms in a layered half-space. *Proceedings of the 4th International Conference "Problems of Geocosmos", St-Petersburg*, 320-323. (In Russian).
- Papageorgiou A.S. and Aki K., (1983) A specific barrier model for the quantitative description of inhomogeneous faulting and the prediction of the strong ground motion. I. Description of the model, *Bull. Seismol. Soc. Am.*, 73, 693-722.
- Somerville, P., K. Irikura, R. Graves, S. Sawada, D. Wald, N. Abrahamson, Y. Iwasaki, T. Kagawa, N. Smith, and A. Kowada (1999). Characterizing crustal earthquake slip models for the prediction of strong motion, *Seism. Res. Lett.* 70, 59–80.
- Wald D.J., Heaton T.H, Hudnut K.W. (1996) The slip history of the 1994 Northridge, California, earthquake determined from strong ground motion, teleseismic, GPS, and leveling data, *Bull. Seism. Soc. Am.*, 86, S49-S70.